Water-Entry of a Wedge with Rolled-up Vortex Sheet

Yuriy A. Semenov[1], and G. X. Wu[1]†

[1]Department of Mechanical Engineering, University College London, London WC1E 6BT, UK

(Received xx; revised xx; accepted xx)

The problem of asymmetric water-entry of a wedge with the vortex sheet shed from its apex is considered within the framework of the ideal and incompressible fluid. The effects due to gravity and surface tension are ignored and the flow therefore can be treated as self similar, as there is no length scale. The solution for the problem is sought through two mutually dependent parts using two different analytic approaches. The first one is due to water entry, which is obtained through the integral hodograph method for the complex velocity potential, in which the streamline on body surface remains on the body surface after passing the apex, leading to a non physical local singularity. The second one is due to vortex sheet shed from the apex, and the shape of the sheet and the strength distribution of the vortex are obtained through the solution of Birkhoff-Rott equation. The total circulation of the vortex sheet is obtained by imposing the Kutta condition at the apex, which removes the local singularity. These two solutions are nonlinearly coupled on the unknown free surface and the unknown vortex sheet. This poses a major challenge, which distinguishes the present formulation of the problem from the previous ones on water entry without vortex sheet and ones on vortex shedding from a wedge apex without a moving free surface. Detailed results in terms of pressure distribution, vortex sheet, velocity and force coefficients are presented for wedges of different inner angles and heel angles, as well as the water entry direction. It is shown that the vortex shedding from the tip of the wedge has profound local effect, but it weakly affects the free surface shape, overall pressure distribution and force coefficients.

1. Introduction

In a wide context, water-entry refers to that in which a solid body penetrates through the free surface of a liquid at large relative speed, in the sense either the body moving towards the liquid or the other way round. This problem has a wide range of applications in many engineering fields. Slamming of marine vehicles, impact of green water on ship decks or offshore platforms and extreme waves including tsunami on the coastline are well-known examples (Faltinsen (2005)). Impact is typically characterized by a short duration, during which velocity and the free surface shape change rapidly both temporally and spatially. It may generate high pressure peaks and large pressure gradients. The severe fluid loading on the structure can lead to its damage or even destruction.

Water entry problems have been extensively investigated using wedge geometry. In addition to direct applications of its results to improve the design of ship hulls, half-submerged propellers, high-speed planing boats and seaplanes etc, the investigations of such a geometry can also reveal some important features and provide better understanding of fluid flows in more general situations. When a symmetric wedge enters a horizontal water surface vertically, the generated flow will be also symmetric, and no flow will cross

† Email address for correspondence: g.wu@ucl.ac.uk

the tip of the wedge. In other cases including asymmetric wedges or oblique entries, the cross flow will occur at the tip of the wedge and the physics of the flow will be changed. Experiments done by Judge et al. (2004) revealed that under certain conditions flow detachment can occur, and this could change flow features completely, especially in the local area. Another important effect of flow asymmetry is that a vortex sheet is shed from the tip, which significantly changes the configuration of the flow near the apex. As in the case without free surface (Pullin (1978), Xu (2016)), the shed vortex leads to the formation of a re-circulation region. These aspects are expected to have some important consequences, especially in the area near the wedge apex. However, these effects have not been carefully considered in the previous works on water entry and they are the main purpose of the present study.

There is a large body of work on water entry of a wedge without taking into account of vortex shedding. The theories based on the incompressible velocity potential for solid-body impact with a liquid were first proposed by von Karman (1929) and Wagner (1932). The former assumed an undisturbed free surface while the latter introduced a correction for the contact point of the body surface and the free surface. Many practical problems have been solved on the basis of these theories. A particular feature in the Wagner theory is that a body is usually replaced by an equivalent plate. The width of the plate is obtained from the horizontal distance between the two contact points of the body with the free surface. It changes with time and needs to be found as part of the solution. The Wagner theory has been found very effective in many cases. However, it predicts an infinite velocity and pressure at the contact point and a jet is usually absent. This drawback has been corrected in further development of the Wagner theory in the framework of the matched asymptotic method. Various impact problems have then been solved through this method by Armand & Cointe (1987), Howison, Ockendon & Wilson (1991), Korobkin & Puknachov (1988), Korobkin (2004), Howison, Ockendon & Oliver (2004) and Oliver (2007). A different modification for the conventional Wagner theory is to take into account the body shape and not to replace it with an equivalent plate as it is done by Zhao, Faltinsen & Aarsnes (1996) using a boundary-integral equation method and Mei, Liu & Yue (1999) using a conformal mapping technique.

Water entry problem has also been solved based on a fully nonlinear model. For a wedge at constant entry speed, when the flow is assumed to be potential, gravity and surface tension effects are ignored, the problem becomes self-similar. Mathematically, the temporal variable can be incorporated into the spatial variables. The boundary conditions on the unknown free surface no longer involves explicitly time but they remain fully nonlinear. The complete solution for such a formulation was obtained by Dobrovol'skaya (1969) for a symmetric wedge entering the free surface vertically. Chekin (1989) generalized Dobrovol'skaya's approach to the problems of the oblique water entry of a wedge and an inclined flat plate. More recently, this problem was considered by Semenov & Iafrati (2006) and Semenov & Yoon (2009), Semenov & Wu (2012) using integral hodograph method (IHM), and by Iafrati (2000) and Xu, Duan & Wu (2008, 2010) using a numerical method. In all these works, the streamline from the tip is attached to the wedge surface and no vortex shedding is taken into account. As a result singularity in velocity and pressure at the wedge apex has appeared. This is obviously a consequence of the pure irrotational flow assumption. In real fluids the streamline will not bend over the corner. Instead, it will separate from the tip and create a re-circulation region. This is obviously due to the viscous effect which is not included in the pure irrotational flow. In order to resolve the velocity singularity at the tip Chekin (1989) proposed a model with the cavity at the tip, however no numerical results were provided. Riccardi & Iafrati (2004) included the pointed vortex shedding from the apex of the wedge during

water entry. However, the free surface was kept flat and the potential on the free surface remained to be zero.

In the present study we address the problem of asymmetric water entry of a wedge with the attached flow on the leeward side and the vortex shedding from the wedge apex. The problem is solved within certain ranges of the wedge heel angle and the direction of the incoming velocity relative the body, confined by some constrains. The first constrain is an obvious geometrical one, which requires that the deadrise angles on both sides of the wedge are positive, or the wedge surface is not in touch with water before the wedge apex does.The second one is the angle between the incoming flow direction and the leeward side of the wedge should not exceed a critical value. Beyond this critical value the liquid will no longer in touch with the surface of the leeward side, or the flow becomes detached, as was observedin experiment by Judge et al (2004). Within these constrains the mathematical model with the fully nonlinear free surface conditions on its exact position together with vortex shedding from the wedge apex is adopted. The vortex shedding is considered in the form of vortex sheet, or vortex line in the present two dimensional case, starting from the wedge apex. The tangential velocity across the vortex line is discontinuous. The total complex velocity potential is split into two components. The first one is principally about the irrotational flow generated by body motion during water entry. The IHM developed previously for free surface flows (Semenov & Wu (2012)) without vortex is used. However, such a solution alone leads to a singularity at the wedge apex. Thus the second part of the solution is due to the vortex sheet started from wedge apex. The method for the vortex sheet follows the formulation of Moore (1975), whose detailed application to a wedge without the free surface was made by Pullin (1978). Unlike the work of Pullin, however, the incoming flow to the wedge here is not a prescribed one but is the one due to water entry. Due to the nonlinearity of the boundary condition, these two components of the problem cannot be solved separately, and they have to be solved simultaneously. In particular, using the dynamic and kinematic boundary conditions on the free surface, the problem is reduced to a system of an integral and an integro-differential equations in the parameter plane, in terms of the velocity magnitude and the velocity angle to the fluid boundary, respectively. The motion of the vortex sheet is governed by Birkhoff-Rott (B-R) integro-differential equation (Rott (1956); Birkhoff (1962)), which expresses the fact that the points of the vortex sheet move with the induced fluid velocity and the corresponding to each of these points the circulation remains unchanged. The coupled systems of equations from the free surface boundary conditions and B-R equations are then solved numerically through successive approximations.

In the following sections the derivation of the integro-differential equations based on IHM and B-R equations are first presented, followed by the numerical method for solving these equations. Results are then provided, in particular near the wedge apex, through the streamlines, vortex-sheet shape, size and location of the re-circulation region and the pressure distribution along the wedge. Discussions are made, including the effects of shedding vortex on the local flow and the free surface, aiming to give some insights into the flow structure and pressure distribution near the wedge apex when the vortex shedding effect is included.

2. Formulation of the problem and the solution procedure

We consider the flow of an ideal incompressible fluid, generated by water entry of a wedge of inner angle 2α. Gravity and surface tension effects are neglected. The pressure on the free surface is assumed to be constant and equal to the atmospheric pressure P_a. The definitions of the geometric parameters are shown in figure 1a. The origin of the

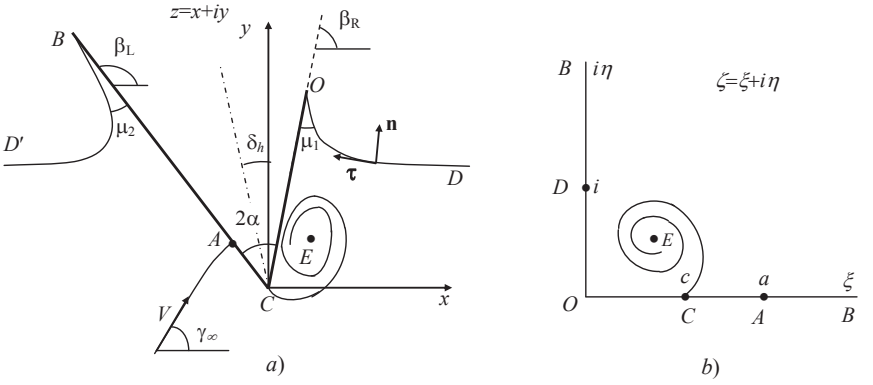

FIGURE 1. (a) Asymmetric water-entry of a wedge: (a) similarity plane $z = x + iy$; (b) the parameter plane.

Cartesian coordinate system xy is fixed at the wedge apex. The liquid is assumed to move toward the stationary solid wedge with velocity V which forms an angle γ_∞ with the x-axis. Then, the free surface elevation at $x = \pm\infty$ approaches $Y_\infty = Vt \sin\gamma_\infty$. The symmetry line of the solid wedge forms a heel angle δ_h with the y-axis. It follows from the geometry of the problem that the right and left sides of the solid wedge form angles $\beta_R = \pi/2 - \alpha + \delta_h$ and $\beta_L = \pi/2 + \alpha + \delta_h$, respectively, with the x-axis. The problem is symmetric only when $\gamma_\infty = 90^\circ$ and $\delta_h = 0$.

A stagnation point A is expected to appear on the windward side of the wedge, where the incoming zero streamline splits into two along the body surface, moving in opposite directions. In the case without vortex sheet (Semenov & Wu (2012)), when the flow moves towards the apex C of the wedge, the liquid accelerates to an infinite speed and turns around the sharp corner. Then, it decelerates on the leeward side. Although such flow configuration is mathematically possible in an ideal fluid, it does not reflect the real physics locally. For real liquid with viscosity, the boundary layer will lead to vorticities shed from the body and both the velocity and pressure at the apex will remain finite. To model this in an ideal liquid, a free shear layer starting from the apex can be introduced (Rott (1956)). Across the layer, the tangential velocity will be discontinuous. The vortex sheet will roll up into a spiral-like shape, as observed in the problem of an infinite wedge in unbounded flow domain (Pullin (1978)).

Here, we will consider the effect of spiral vortex effect during water entry. The problem is self-similar since there is no length scale. Therefore, the time-dependent problem in the physical plane $Z = X + iY$ can be written in the stationary plane $z = x + iy$ in terms of the self-similar variables $x = X/(Vt)$ and $y = Y/(Vt)$, where t is time starting from the moment of impact. The complex velocity potential $W(Z,t) = \Phi(Z,t) + iY(Z,t)$ for the self-similar flow is written in the form

$$W(Z,t) = V^2 t w(z) = V^2 t \left[\phi(x,y) + i\psi(x,y)\right]. \tag{2.1}$$

where $\phi(x,y)$ and $\psi(x,y)$ are the velocity potential and the stream function in the similarity plane. We may decompose the complex potential of such flow into two components

$$w(z) = w_1(z) + w_2(z), \tag{2.2}$$

where $w_1(z)$ is the complex potential due to water entry without vortex sheet and $w_2(z)$ is the complex potential due to the spiral vortex sheet. The complex potential $w_1(z)$ has singularity at the apex of the wedge. Introduction of the complex potential $w_2(z)$ is to

ensure that there will be no singularity in $w(z)$, and the velocity at the apex will be finite. This means that a singularity at point C exists in $w_2(z)$, which has the same order as that in $w_1(z)$.

2.1. *General approach for solving free surface problems.*

In order to determine the function $w(z)$ we introduce a parameter plane, or zeta -plane, as suggested by Joukovskii (1890) and Michell (1890). Then, the complex velocity, or strictly speaking the conjugate of the complex velocity, dw/dz, and the derivative of the complex potential, $dw/d\zeta$, are found as the functions of the parameter zeta in the form as

$$w(\zeta) = w(0) + \int_0^\zeta \frac{dw}{d\zeta} d\zeta, \qquad z(\zeta) = z(0) + \int_0^\zeta \frac{dw}{d\zeta} \Big/ \frac{dw}{dz} d\zeta. \tag{2.3}$$

Further development of this method was done by Chaplygin (see chapter 4 in Gurevich (1965)), who suggested to analyse singular points of a complex function and then to find it using Liouville's theorem, instead of using the conformal mapping in an explicit form. We choose the first quadrant of the ζ-plane as the parameter region corresponding to the physical domain to derive expressions for the complex velocity, dw/dz, and the derivative of the complex potential, $dw/d\zeta$, as functions of the variable $\zeta = \xi + i\eta$. Conformal mapping allows us to fix three points in the parameter region arbitrarily, which are chosen as O, B and D in the present problem, as shown in figure 1*b*. The first two are the intersections of the free surface with the body surface and the last one is at infinity. In this parameter plane, the positive imaginary axis ($\eta > 0$, $\xi = 0$) corresponds to the free surface, and the positive real axis ($\xi > 0$, $\eta = 0$) corresponds to the wetted part of the wedge. The points $\zeta = a$ and $\zeta = c$ are the images of the stagnation point A and the wedge apex C in the similarity plane, respectively. The values of a and c are not known and have to be determined as part of the solution.

According to (2.2), we may write

$$\frac{dw}{dz} = \frac{dw_1}{dz} + \frac{dw_2}{dz} = \frac{dw_1}{dz} F(z), \tag{2.4}$$

$$\frac{dw}{d\zeta} = \frac{dw_1}{d\zeta} + \frac{dw_2}{d\zeta} = \frac{dw_1}{d\zeta} F(z), \tag{2.5}$$

where

$$F(\zeta) = \left(1 + \frac{dw_2}{dz} \Big/ \frac{dw_1}{dz}\right) = \left(1 + \frac{dw_2}{d\zeta} \Big/ \frac{dw_1}{d\zeta}\right). \tag{2.6}$$

This indicates that the potential w_1 is chosen as the reference potential, as dw_1/dz and $dw_1/d\zeta$ can be obtained from the solution of the problem without vortex sheet (Semenov & Wu (2012). Moreover, from (2.4) and (2.5) it follows that the derivative of the mapping function,

$$\frac{dz}{d\zeta} = \frac{dw}{d\zeta} \Big/ \frac{dw}{dz} = \frac{dw_1}{d\zeta} \Big/ \frac{dw_1}{dz} \tag{2.7}$$

is directly linked to the reference potential w_1 only.

In order to derive an expression for the derivative of the complex potential, $dw/d\zeta$, we analyse the behaviour of the velocity potential along the free surface. It is useful to introduce the unit vectors $\boldsymbol{n}$ and $\boldsymbol{\tau}$ in the normal and tangential directions of the fluid boundary, respectively. The normal vector points out of the fluid region while the spatial arc length coordinate s along the surface increases in the direction of $\boldsymbol{\tau}$, along which the

fluid region is on the left (figure 1a). With this notation,

$$dw = (v_s + iv_n)ds, \tag{2.8}$$

where v_s and v_n are the tangential and normal velocity components, respectively. Let θ be the angle between the velocity vector on the surface and $\boldsymbol{\tau}$, which means $\theta = \arg(v_s + iv_n)$. Taking the magnitude of (2.4) and the argument of equation

$$\frac{dw}{ds} = \frac{dw_1}{ds} + \frac{dw_2}{ds} = \frac{dw_1}{ds} F(\zeta),$$

we can obtain

$$v(\eta) = \left|\frac{dw}{dz}\right|_{\zeta=i\eta} = v_1(\eta) v_F(\eta), \tag{2.9}$$

$$\theta(\eta) = \arg\left(\frac{dw}{ds}\right) = \arg\left(\frac{dw_1}{ds}\right) + \arg[F(\zeta)_{\zeta=i\eta}] = \theta_1(\eta) + \theta_F(\eta), \tag{2.10}$$

where

$$v_1(\eta) = \left|\frac{dw_1}{dz}\right|_{\zeta=i\eta}, \quad \theta_1(\eta) = \arg\left(\frac{dw_1}{ds}\right)_{\zeta=i\eta},$$
$$v_F(\eta) = |F(\zeta)|_{\zeta=i\eta}, \quad \theta_F(\eta) = \arg\left[F(\zeta)\right]_{\zeta=i\eta}.$$

2.2. *Complex potential due to water entry.*

The problem of impact between the liquid wedge and solid wedge without vortex sheet, in which a singularity exits at the wedge apex, has been solved by Semenov & Wu (2012). There the expressions for the complex velocity and the derivative of the complex potential as well as the mapping function $z = z(\zeta)$ were derived, and the flat free surface problem was treated as a special case of a liquid wedge with an inner angle π. In the present notations, the expression for the complex velocity, dw_1/dz, takes the form

$$\frac{dw_1}{dz} = v_0 \left(\frac{\zeta - a}{\zeta + a}\right) \left(\frac{\zeta + c}{\zeta - c}\right)^{1-2\alpha/\pi} \exp\left[-\frac{i}{\pi}\int_0^\infty \frac{d\ln v_1}{d\eta} \ln\left(\frac{i\eta - \zeta}{i\eta + \zeta}\right) d\eta - i\beta_L\right], \tag{2.11}$$

where $v_0 = v(\eta)_{\eta=0}$ is the velocity magnitude at point O. It can be clearly seen that the complex velocity has a singularity of the order $(\zeta - c)^{2\alpha/\pi - 1}$ at point $\zeta = c$ which corresponds to the wedge apex. Through analysing the behaviour of the angle of the velocity, $\theta_1 = \arg(v_s + iv_n)$, relative to the boundary, the derivative of the complex potential, $dw_1/d\zeta$, was obtained in the form

$$\frac{dw_1}{d\zeta} = K\zeta^{2\mu_1/\pi - 1} \frac{\zeta^2 - a^2}{(\zeta + 1)^2} \exp\left[\frac{1}{\pi}\int_0^\infty \frac{d\theta_1}{d\eta} \ln\left(\zeta^2 + \eta^2\right) d\eta\right], \tag{2.12}$$

where K is a real factor.

From (2.11) and (2.12) the derivative of the mapping function can be obtained as

$$\frac{dz}{d\zeta} = \frac{K}{v_0}\zeta^{2\mu_1/\pi - 1} \frac{(\zeta + a)^2}{(1 + \zeta)^2} \left(\frac{\zeta - c}{\zeta + c}\right)^{1-2\alpha/\pi} \exp\left[\frac{1}{\pi}\int_0^\infty \frac{d\theta_1}{d\eta} \ln\left(\eta^2 + \zeta^2\right) d\eta\right.$$
$$\left. + \frac{i}{\pi}\int_0^\infty \frac{d\ln v_1}{d\eta} \ln\left(\frac{i\eta - \zeta}{i\eta + \zeta}\right) d\eta + i\beta_L\right]. \tag{2.13}$$

(2.11) - (2.13) contain the parameters a, c, K and the functions $v_1(\eta)$ and $\theta_1(\eta)$, which are to be determined from physical considerations and the dynamic and kinematic boundary conditions on the free surface. At infinity, the complex velocity tends to $\exp(-i\gamma_\infty)$. Taking the argument of (2.4) and accounting for (2.11), we have

$$\arg\left(\frac{dw}{dz}\right)_{\zeta=i} = \arg\left(\frac{dw_1}{dz}\right)_{\zeta=i} + \arg[F(\zeta)]_{\zeta=i} = \arg\left(\frac{dw_1}{dz}\right)_{\zeta=i} + \theta_F(\eta)_{\eta=1} = -\gamma_\infty.$$

By letting $\zeta = i$ in (2.11), which corresponds to infinity in the self similar plane, the following equation is obtained

$$-2\tan^{-1}\frac{1}{a}+\left(2-\frac{4\alpha}{\pi}\right)\tan^{-1}\frac{1}{c}-\frac{1}{\pi}\int_0^\infty \frac{d\ln v_1}{d\eta}\ln\left|\frac{\eta-1}{\eta+1}\right|d\eta+\theta_F(1)+\alpha-\delta_h-\frac{\pi}{2}+\gamma_\infty = 0. \tag{2.14}$$

In the physical plane, the wetted length of the right side of the wedge in the self similar flow is $v_0 Vt$. The length of the segment OC in the similarity plane is then $|z_O| = v_0$. Hence, the following equation is obtained

$$\int_0^c \left|\frac{dz}{d\zeta}\right|_{\zeta=\xi} d\xi = v_0. \tag{2.15}$$

An additional condition is obtained by enforcing the fact that the $y-$coordinates of the free surface on the right- and left-hand sides have to be the same at infinity. This gives

$$\Im\left(\oint_{\zeta=i}\frac{dz}{d\zeta}d\zeta\right) = \Im\left(\pi i \operatorname*{Res}_{\zeta=i}\frac{dz}{d\zeta}\right) = \Im\left[\pi i \lim_{\zeta\to i}\frac{d}{d\zeta}\left(\frac{dz}{d\zeta}(\zeta-i)^2\right)\right] = 0.$$

By taking into account (2.13) and performing the integration through the residue method we get

$$-\left(\frac{\mu_1}{\pi}-1\right)-\frac{1}{1+a^2}+\frac{1}{\pi}\int_0^\infty \frac{d\theta_1}{d\eta}\frac{d\eta}{\eta^2-1} = 0. \tag{2.16}$$

From (2.14) - (2.16) the parameters a, c, K can be found if the functions $v_1(\eta)$ and $\theta_1(\eta)$ are specified.

2.2.1. *Dynamic boundary condition on the free surface.*

The Bernoulli equation in the physical plane linking point O and an arbitrary point in the flow domain gives

$$\left.\frac{\partial\Phi}{\partial t}\right|_Z + \frac{V'^2}{2}+\frac{P}{\varrho} = \left.\frac{\partial\Phi}{\partial t}\right|_{Z=0} + \frac{V_0^2}{2}+\frac{P_a}{\varrho}\quad . \tag{2.17}$$

where P and V' are the pressure and velocity at the arbitrary point of the fluid domain, ϱ is the density of the liquid. By taking advantage of self-similarity of the flow defined in (2.1), and using the spatial coordinate of arc length, $s = S/(Vt)$, Semenov & Iafrati (2006) reduced this equation to the following

$$v_*^2 - v^2 - 2(\phi-\phi_*) + 2\frac{d\phi}{ds}s = 0 \tag{2.18}$$

Here, the subscript $*$ together with $s = 0$ refers to the intersection points O and B respectively for the right and left free surfaces. By taking the derivative of (2.18) with respect to s, and using $d\phi/ds = v_s$ and $v_s = v\cos\theta$, the following differential equation is obtained

$$\frac{d\theta}{ds} = \frac{v+s\cos\theta}{s\sin\theta}\frac{d\ln v}{ds}\quad . \tag{2.19}$$

Multiplying both sides of (2.19) by $ds/d\eta$ and taking into account that $\theta(\eta) = \theta_1(\eta) + \theta_F(\eta)$, $v(\eta) = v_1(\eta)v_F(\eta)$, we obtain the following integro-differential equation:

$$\frac{d\theta_1}{d\eta} = \frac{v_1 v_F + s\cos(\theta_1+\theta_F)}{s\sin(\theta_1+\theta_F)}\left(\frac{d\ln v_1}{d\eta} + \frac{d\ln v_F}{d\eta}\right) - \frac{d\theta_F}{d\eta} \quad . \tag{2.20}$$

where the arc length coordinate $s = s(\eta)$ can be obtained by integrating (2.13)

$$s(\eta) = -\int_0^\eta \left|\frac{dz}{d\zeta}\right|_{\zeta=i\eta'} d\eta' = -K\int_0^\eta \frac{\eta'^{(2\mu_1-1)}}{v_1(\eta')}\frac{\eta'^2+a^2}{(1-\eta'^2)^2} \times \exp\left[\frac{1}{\pi}\int_0^\infty \frac{d\theta_1}{d\eta''}\ln\left|\eta''^2-\eta'^2\right| d\eta''\right] d\eta', \qquad 0<\eta<1, \tag{2.21}$$

for the free surface on the right hand side and

$$s(\eta) = \int_\eta^\infty \left|\frac{dz}{d\zeta}\right|_{\zeta=i\eta'} d\eta', \qquad 1<\eta<\infty, \tag{2.22}$$

for the free surface on the left hand side.

2.2.2. *Kinematic boundary condition on the free surface.*

The kinematic boundary condition in terms of the velocity magnitude v and angle $\beta = -\arg(dw/dz)$ for this kind of self-similar flow problem has the following form Semenov & Iafrati (2006)

$$\frac{1}{\tan\theta}\frac{d\ln v}{ds} = \frac{d}{ds}\left[\arg\left(\frac{dw}{dz}\right)\right]. \tag{2.23}$$

This equation is obtained using the fact that the acceleration of the fluid particle is orthogonal to the free boundary of constant pressure. Substituting the complex velocity in (2.11) into (2.23) and multiplying both sides of the result by $ds/d\eta = |dz/d\zeta|_{\zeta=i\eta}$, the following integral equation for the function $d\ln v_1/d\eta$ is obtained

$$-\frac{1}{\tan(\theta_1+\theta_F)}\frac{d\ln v_1}{d\eta} + \frac{1}{\pi}\int_0^\infty \frac{d\ln v_1}{d\eta'}\frac{2\eta'}{\eta'^2-\eta^2}d\eta' = \frac{1}{\tan(\theta_1+\theta_F)}\frac{d\ln v_F}{d\eta} - \frac{d\theta_F}{d\eta} + \frac{2a}{a^2+\eta^2} + \left(\frac{2\alpha}{\pi}-1\right)\frac{2c}{c^2+\eta^2}\,. \tag{2.24}$$

The integral equations (2.20) and (2.24) together with equations (2.14), (2.15) and (2.16) make it possible to determine the functions $\theta_1(\eta)$ and $v_1(\eta)$, and the parameters a, c and K if the functions $\theta_F(\eta)$ and $v_F(\eta)$ are known. Once these functions are found, the contact angles between the wedge sides and the free surface, μ_1 and μ_2 can be determined as follows:

$$\mu_1 = \lim_{\eta\to 0}\theta_1(\eta), \qquad \mu_2 = \pi - \lim_{\eta\to\infty}\theta_1(\eta). \tag{2.25}$$

The former is explicitly required in the expression for the derivative of the complex potential in (2.12).

2.3. *Complex potential of the vortex sheet.*

We consider the vortex sheet as a cut in the fluid domain. The liquid on both sides of the cut has the same normal velocity component but their tangential components are different. Similar to that proposed by Moore (1975), we describe the position of the vortex sheet in the similarity plane by a complex function $Z_0(\Gamma, t)$, where Γ is the circulation obtained by integration of the vortex strength from the centre of the spiral

(point E in figure 1a) to point Z_0, and $\Gamma = \Gamma_C$ at point C is the total circulation. This formulation has made use of the fact that point Z_0 can be written as a function of Γ, as when Z_0 is followed, since $d\Gamma/dt = 0$ (e.g., p.30, Saffman (1993)), or Z_0 always corresponds to the same Γ. We may introduce the parameter $\lambda = 1-\Gamma/\Gamma_C$ which changes from $\lambda = 0$ at point C to $\lambda = 1$ at point E. Then, the vortex sheet in the similarity plane can be written as $z_0(\lambda) = Z_0/(Vt)$. The line $\zeta_0(\lambda)$ is the image of the vortex sheet $z_0(\lambda)$ in the parameter plane.

We will build such an expression for the complex potential $w_2(\zeta)$ whose imaginary part equals zero along the real and imaginary axes of the parameter plane. Then, the normal velocity due to $w_2(\zeta)$ on the fluid boundary is zero, which means that the required impermeable condition on the wedge surface is satisfied.

A concentrated vortex of circulation γ^* at point $\zeta_0 = \xi_0 + i\eta_0$ in the parameter plane creates the logarithmic complex potential $w^*(\zeta,\zeta_0) = \gamma^*/(2\pi i)\ln(\zeta-\zeta_0)$. Due to the simple geometry of the parameter region, we can obtain the potential $w^*_{total}(\zeta,\zeta_0)$ which has constant imaginary part along the positive real and imaginary axes by adding the image vortexes of the same strength at points $-\zeta_0$, $\overline{\zeta_0}$ and $-\overline{\zeta_0}$, or

$$w^*_{total}(\zeta,\zeta_0) = w^*(\zeta,\zeta_0) + w^*(\zeta,-\zeta_0) + w^*(\zeta,\overline{\zeta_0}) + w^*(\zeta,-\overline{\zeta_0})$$

For vortex distribution γ' along a segment ds, γ^* in the above equation can be replaced by $\gamma' ds$. Following this principle, the sheet with varying strength, the complex potential can be written as

$$w_2(\zeta) = -\frac{J}{2\pi i}\int_0^1 \left\{\ln\left[\zeta-\zeta_0(\lambda)\right] - \ln\left[\zeta-\overline{\zeta_0}(\lambda)\right] - \ln\left[\zeta+\overline{\zeta_0}(\lambda)\right] + \ln\left[\zeta+\zeta_0(\lambda)\right]\right\} d\lambda \tag{2.26}$$

in which $d\lambda = -\gamma' ds$ has been used and therefore the integration is performed with respect to λ. This gives

$$\frac{dw_2}{d\zeta} = -\frac{J}{2\pi i}\int_0^1 \left(\frac{1}{\zeta-\zeta_0(\lambda)} - \frac{1}{\zeta-\overline{\zeta_0}(\lambda)} - \frac{1}{\zeta+\overline{\zeta_0}(\lambda)} + \frac{1}{\zeta+\zeta_0(\lambda)}\right) d\lambda, \tag{2.27}$$

where $J = \Gamma_C/(V^2 t)$. It is well known that the right-hand side of (2.27) is discontinuous across the vortex sheet. It takes different values according to the Plemelj formula

$$\left.\frac{dw_2}{d\zeta}\right|_{\zeta=\zeta_0(\lambda)} = -J\left[\pm\frac{1}{2}\left(\frac{d\zeta_0}{d\lambda}\right)^{-1} + \frac{1}{2\pi i}P\int_0^1 \left(\frac{1}{\zeta-\zeta_0(\lambda)} - \frac{1}{\zeta-\overline{\zeta_0}(\lambda)} - \frac{1}{\zeta+\overline{\zeta_0}(\lambda)} + \frac{1}{\zeta+\zeta_0(\lambda)}\right) d\lambda\right], \tag{2.28}$$

as a point $\zeta_0(\lambda)$ on the sheet is approached by ζ from the $\pm$ side. Symbol P in (2.28) indicates the Cauchy principal value integral.

2.4. *Kutta condition.*

From (2.4) and (2.11) it can be seen that complex velocity has a singularity of the form $(\zeta-c)^{2\alpha/\pi-1}$ as $\zeta \to c$,

$$\frac{dw}{d\zeta} = \left(\frac{dw_1}{d\zeta} + \frac{dw_2}{d\zeta}\right)\Big/\frac{dz}{d\zeta} = \frac{(\zeta-c)^{2\alpha/\pi-1}}{f_z(\zeta)}\left(\frac{dw_1}{d\zeta} + \frac{dw_2}{d\zeta}\right), \quad 0<\alpha<\pi/2, \tag{2.29}$$

where $f_z(\zeta) = (\zeta-c)^{2\alpha/\pi-1} dz/d\zeta$ is an analytical function at point $\zeta = c$. This singularity in the complex velocity is to be removed by the vortex sheet, which leads to a finite value

of dw/dz as $\zeta \to c$. Therefore, substituting (2.27) into (2.28), we should impose

$$\left.\frac{dw_1}{d\zeta}\right|_{\zeta=c} - \frac{J}{2\pi i} P\int_0^1 \left(\frac{1}{c-\zeta_0(\lambda)} - \frac{1}{c-\overline{\zeta_0}(\lambda)} - \frac{1}{c+\overline{\zeta_0}(\lambda)} + \frac{1}{c+\zeta_0(\lambda)}\right) d\lambda = 0\,. \quad (2.30)$$

This is the well-known Kutta condition from which the total circulation, J, is determined.

2.5. *Birkhoff - Rott integral equation for the evolution of the vortex sheet.*

Following the formulation of Moore (1975) and also that in Pullin (1978), the equation of motion of the two-dimensional vortex sheet, $Z_0(\Gamma, t)$, in the physical plane is

$$\left.\frac{\partial \overline{Z}_0}{\partial t}\right|_{\Gamma} = \frac{1}{2}\left[\left(\frac{\partial W}{\partial Z}\right)^{+} + \left(\frac{\partial W}{\partial Z}\right)^{-}\right], \quad (2.31)$$

in which the left hand side is the Lagrangian velocity of the sheet and the right hand side is the induced Eulerian complex velocity at the same point Z_0. It differs from the complex velocity of the liquid particles at the point Z_0 on both sides of the sheet. In other words, the induced velocity of the sheet equals the average of local particle velocities on both sides of the sheet. As the vortex strength remains constant when following the movement of the same point Z_0 on the vortex sheet, (2.31) automatically satisfies the continuity conditions of normal velocity and pressure across the sheet Saffman (1993). Substituting $z_0(\lambda) = Z(\Gamma, t)/(Vt)$ and $w = W/(V^2 t)$ into (2.31), we have in the similarity plane

$$\overline{z}_0(\lambda) + (1-\lambda)\frac{d\overline{z_0}}{d\lambda} = \left(\frac{dw}{dz}\right)_{ind}, \quad (2.32)$$

where

$$\left(\frac{dw}{dz}\right)_{ind} = \frac{(\zeta_0(\lambda)-c)^{2\alpha/\pi-1}}{f_z[\zeta_0(\lambda)]}\left(\left.\frac{dw_1}{d\zeta}\right|_{\zeta=\zeta_0}\right. \quad (2.33)$$

$$\left. - \frac{J}{2\pi i} P\int_0^1 \left(\frac{1}{\zeta_0(\lambda)-\zeta_0(\lambda')} - \frac{1}{\zeta_0(\lambda)-\overline{\zeta_0}(\lambda')} - \frac{1}{\zeta_0(\lambda)+\overline{\zeta_0}(\lambda')} + \frac{1}{\zeta_0(\lambda)+\zeta_0(\lambda')}\right) d\lambda'\right),$$

and $f_{z0}(\zeta_0) = f_z(\zeta)_{\zeta=\zeta_0}$ is the average speed corresponding to right hand side of (2.32) in the self similar plane. This integro-differential equation will then be solved in the parameter plane in which the shape of the vortex sheet z_0 is written as $z_0[\zeta_0(\lambda)]$.

(2.33) contains a singular factor $(\zeta_0(\lambda)-c)^{2\alpha/\pi-1}$. However, due to the Kutta condition in (2.30), the complex velocity at the wedge apex is finite when approaching on the windward side, and is zero on the leeward side, which will be shown later. (2.30) and (2.32) determine the circulation and the shape of the vortex sheet, which subsequently completely determines the derivative of the complex potential, $dw_2/d\zeta$. Thus, it gives a closed system of equations derived in section 2.2 for the problem of water-entry of the wedge with the vortex sheet.

2.6. *Leading order of the B-R equation at the wedge apex.*

In order to determine velocities of the liquid on both the windward and leeward sides of the sheet near the wedge apex, we consider the leading order of (2.32). Following Rott (1956) and Pullin (1978), we use (2.30) to replace $(dw_1/d\zeta)_{\zeta=c}$ and to rewrite (2.32)

and (2.33) in the following form

$$\overline{z}_0(\lambda) + (1-\lambda)\frac{d\overline{z_0}}{d\lambda} = \frac{(\zeta_0(\lambda)-c)^{2\alpha/\pi}}{f_z[\zeta_0(\lambda)]} \tag{2.34}$$
$$\times \frac{J}{2\pi i}\left\{P\int_0^1 \left(\frac{1}{[c-\zeta_0(\lambda')][\zeta_0(\lambda)-\zeta_0(\lambda')]} - \frac{1}{[c-\overline{\zeta_0}(\lambda')][\zeta_0(\lambda)-\overline{\zeta_0}(\lambda')]}\right)d\lambda'\right.$$
$$\left. + \int_0^1 \left(-\frac{1}{[c+\overline{\zeta_0}(\lambda')][\zeta_0(\lambda)-\overline{\zeta_0}(\lambda')]} + \frac{1}{[c+\zeta_0(\lambda')][\zeta_0(\lambda)+\zeta_0(\lambda')]}\right)d\lambda'\right\}$$

Here, the terms in the integrand have been combined and as a result the term $(\zeta-c)^{-1}$ has been cancelled in the equation. We also notice that the second integral is non-singular.

Near $\zeta_0 = c$ or $\lambda = 0$, we seek a solution valid to the leading order of λ, which we assume is of the form similar to that in Pullin (1978)

$$\zeta_0 = c + K^*\lambda^\mu + \textit{higher order terms} \tag{2.35}$$

where K^* is a complex constant and $\mu > 0$. Then, keeping the leading orders in λ on the left and right hand sides of (2.34) and focusing attention on the first integral containing the singular terms, we obtain

$$\frac{dz_0}{d\zeta_0}\frac{\overline{d\zeta_0}}{d\lambda} = \frac{(\zeta_0(\lambda)-c)^{2\alpha/\pi}}{f_z(\zeta_0)} JG[\zeta_0(\lambda)], \tag{2.36}$$

where $dz_0/d\zeta_0 = dz/d\zeta|_{\zeta=\zeta_0}$ and

$$G[\zeta_0(\lambda)] = -\frac{J}{2\pi i}P\int_0^1 \left(\frac{1}{[c-\zeta_0(\lambda')][\zeta_0(\lambda)-\zeta_0(\lambda')]} - \frac{1}{[c-\overline{\zeta_0}(\lambda')][\zeta_0(\lambda)-\overline{\zeta_0}(\lambda')]}\right)d\lambda'. \tag{2.37}$$

Substituting $\lambda = \lambda(\zeta_0)$ from (2.35) in (2.37), the two integrals can be written as below

$$\int_0^{\zeta^*} \frac{d\lambda}{d\zeta_0'}\frac{d\zeta_0'}{(\zeta_0'-c)(\zeta_0'-c-(\zeta_0-c))} = \frac{1}{\mu}\left(\frac{1}{K^*}\right)^{\frac{1}{\mu}}\int_0^{\zeta_c^*}\frac{d\zeta_c'}{{\zeta_c'}^{2-\frac{1}{\mu}}(\zeta_c'-\zeta_c)}, \tag{2.38}$$

$$\int_0^{\zeta^*} \frac{d\lambda}{\overline{d\zeta_0'}}\frac{\overline{d\zeta_0'}}{(\overline{\zeta_0'}-c)(\overline{\zeta_0'}-c-(\zeta_0-c))} = \frac{1}{\mu}\left(\frac{1}{\overline{K^*}}\right)^{\frac{1}{\mu}}\int_0^{\zeta_c^*}\frac{d\overline{\zeta_c'}}{\overline{\zeta_c'}^{2-\frac{1}{\mu}}(\overline{\zeta_c'}-\zeta_c)}, \tag{2.39}$$

where $\zeta_c = \zeta_0 - c$, $\zeta_c^* = \zeta^* - c$ and ζ^* is close to c since we consider the leading order and use (2.35). Following Gakhov (1990) the leading order of the function $G(\zeta_0)$ can be obtained as

$$G(\zeta_0) = \frac{1}{2i\mu}(\zeta_0-c)^{1/\mu-2}\left\{\cot\left[(2-1/\mu)\,\pi\right]\left(\frac{1}{K^*}\right)^{1/\mu}\right.$$
$$\left. - \frac{\exp\left[-i\,(2-1/\mu)\,\pi\right]}{\sin\left[(2-1/\mu)\,\pi\right]}\left(\frac{1}{\overline{K}^*}\right)^{1/\mu}\right\} + G^*(\zeta_0) \tag{2.40}$$

where $(\zeta_0-c)^{2-1/\mu}G^*(\zeta_0) \to 0$ for $\zeta_0 \to c$. The first term in curl brackets of (2.40) corresponds to (2.38) and the second to (2.39). Substituting this result into (2.36), using (2.35) and (2.13) and equating powers of the leading order in λ we can obtain $1/\mu = 2(1-\alpha/\pi)$ and

$$K^* = \left[\frac{2J(1-\alpha/\pi)^2}{|f_z(\zeta)_{\zeta=c}|^2}\right]^{\frac{1}{4-4\alpha/\pi}} \times \exp\left(\frac{i\pi}{2-2\alpha/\pi}\right). \tag{2.41}$$

Substitution of (2.41) into (2.30) gives

$$G(\zeta_0) = \frac{1}{\sqrt{2J}}(\zeta_0 - c)^{-2\alpha/\pi}\,|f_z(\zeta_0)| + G^*(\zeta_0). \tag{2.42}$$

The complex velocity on the $\pm$ sides of the vortex sheet near $\zeta = c$, given by (2.29) can be expressed in terms of function $G(\zeta_0)$

$$\left(\frac{dw}{d\zeta}\right)^{\pm} = \frac{(\zeta - c)^{2\alpha/\pi - 1}}{f_z(\zeta_0)} J \left[\pm\frac{1}{2}\left(\frac{d\zeta_0}{d\lambda}\right)^{-1} + (\zeta_0 - c)G(\zeta_0)\right]. \tag{2.43}$$

By using (2.35) and (2.41), the first term in the brackets can be determined as $(d\zeta_0/\lambda)^{-1} = -(\zeta_0 - c)^{1-2\alpha/\pi}|f_z(\zeta_0)|\sqrt{2/J}$. Substituting this into (2.43), we obtain velocity near the apex on the leeward and windward sides of the wedge respectively as

$$\left(\frac{dw}{d\zeta}\right)^{+} = \frac{(\zeta_0 - c)^{2\alpha/\pi}}{f_z(\zeta_0)} JG^*(\zeta_0), \tag{2.44}$$

$$\left(\frac{dw}{d\zeta}\right)^{-} = \sqrt{\frac{2}{J}}\frac{|f_z(\zeta_0)|}{f_z(\zeta_0)} + \frac{(\zeta_0 - c)^{2\alpha/\pi}}{f_z(\zeta_0)} JG^*(\zeta_0) = \sqrt{2J}\exp^{-i\beta_L} + \frac{(\zeta_0 - c)^{2\alpha/\pi}}{f_z(\zeta_0)} JG^*(\zeta_0). \tag{2.45}$$

From (2.44) it follows that the leeward side of the wedge apex is a stagnation point while the non-dimensional speed on the windward side is $\sqrt{2J}$. This result in fact satisfies the Bernoulli equation. From (2.45) it can also be seen that the vortex sheet leaves the wedge apex tangentially to the windward surface, as found by others for similar problems Pullin (1978), Jones (2003).

The leading-order of the function $\zeta_0 = \zeta_0(\lambda)$ for small λ is

$$\zeta_0(\lambda) = c + \left[\frac{2J(1 - \alpha/\pi)^2}{|f_z(\zeta)_{\zeta=c}|^2}\right]^{1/(4-4\alpha/\pi)} \exp^{i\pi/(2-2\alpha/\pi)}\,\lambda^{1/(2-2\alpha/\pi)} + \cdots. \tag{2.46}$$

which is to be used to determine position of the first node in numerical solution of the integral equation (2.32), as discussed below.

3. Results and discussion

3.1. *Numerical method*

The system of equations derived in section 2 is solved numerically by iteration through the method of successive approximations. By following the formulation of the problem, the numerical procedure divides equations into two blocks. The first block contains (2.14) - (2.16) and integral equations (2.20) and (2.24) determining the flow potential $w_1(\zeta)$ at a given potential of the vortex sheet, $w_2(\zeta)$. The second block contains (2.30) and (2.33), (2.34) determining the flow potential of the vortex sheet, $w_2(\zeta)$, at a given potential $w_1(\zeta)$. It has been found in the calculation that starting with $w_2(\zeta) \equiv 0$, $5 - 10$ iterations are usually required between these two blocks to reach a tolerance of $\max|\lambda(s)^{k+1} - \lambda(s)^k| < 10^{-4}$ between two successive iterations, where s is the arc length variable along the vortex sheet.

The first block of equations including integral equations (2.20) and (2.24) are solved numerically through an internal iteration procedure. Conditions in (2.14), (2.15) and (2.16) are imposed at each iteration. In discrete form, the solution is sought on two sets of points. The first set, $0 < \eta_j \leqslant 1$, $j = 1, ..., N$, corresponds to the segment OD of the free surface and the points are distributed in such a way, that the segment size increases

geometrically away from O. The second set of points $1 < \eta_j < \eta_{2N}$, $j = N+1, ..., 2N$, corresponding to BD, is chosen in similar way starting from point B. Typical values $\eta_1 = 10^{-5}$ and $\eta_{2N} = 10^5$ are chosen. The successive approximations used here follow those in Semenov & Iafrati (2006) and Semenov & Wu (2012) for solving self-similar water entry problems without vortex sheet.

The solution at the intersection of the free surface and body surface is computationally very challenging due to the singularity in the derivative of the complex potential at point O ($\eta = 0$) with the order $2\mu_1/\pi - 1 < 0$, as can be seen in (2.12), and due to the improper integral with upper limit at $\eta = \infty$ corresponding to point B. The singular natures at these intersection points depend on the values of the contact angles μ_1 and μ_2, respectively, which in turn depend on the function $\theta(\eta)$, or its limits at $\eta \to 0$ and $\eta \to \infty$, respectively. For a given discretisation along the $\eta-$axis discussed above, the corresponding arc length coordinates $s_1 = s(\eta_1)$ and $s_{2N} = s(\eta_{2N})$ nearest to contact points O and B in the similarity plane can be obtained using (2.21) and (2.22), respectively as

$$s_1 = -\pi K a^2 \exp\left(\frac{2}{\pi}\int_{\eta_1}^{\eta_{2N}} \frac{d\theta_1}{d\eta}\ln\eta d\eta\right)\frac{\eta_1^{2\mu_1/\pi}}{2v_0\mu_1} \tag{3.1}$$

$$s_{2N} = \pi K \frac{\eta_{2N}^{-2\mu_2/\pi}}{2v_B\mu_2} \tag{3.2}$$

where v_B is the velocity magnitude at point B. Then, the arc length coordinates $s_j = s(\eta_j)$, $j = 2, ..., 2N-1$ are obtained by using (2.21) and (2.22).

(2.32) in the second block of equations is the integral equation with respect to complex function $\zeta_0(\lambda)$ determining the vortex sheet location in the parametric plane, and in the similarity plane $z_0 = z[\zeta_0(\lambda)]$. (2.32) also determines the circulation distribution along this line. It is a rather complex problem to solve (2.32) and (2.33) directly. Instead we split this equation in the complex domain into two equations in real domain. For this purpose, it is useful to introduce the angle

$$\delta_v = \beta_v + \theta_v, \tag{3.3}$$

where δ_v is the slope of the vortex line, $\beta_v = -\arg(dw/dz)_{\zeta=\zeta_0(\lambda)}$ is the angle of the induced velocity to the $x-$axis obtained from (2.33) and θ_v is the angle of the induced velocity to the vortex line. By using the fact that $dw/ds = v_\tau + iv_n$ and $dz/ds = \exp(i\delta_v)$, the induced velocity can be presented in terms of its tangential and normal components as follows

$$e^{i\delta_v}\left(\frac{dw}{dz}\right)_{ind} = v_\tau + iv_n \tag{3.4}$$

By multiplying the left hand side of (2.32) $e^{i\delta_v}$ and separating the real and imaginary parts, we can obtain the following equation

$$\frac{d\lambda}{ds} = \frac{1-\lambda}{v_\tau - \Re(\overline{z_0}e^{i\delta_v})}, \tag{3.5}$$

and the equation for the angle of the induced velocity to the vortex line

$$\theta_v = \arctan\left(\frac{v_n}{v_\tau}\right) = \arctan\left(\frac{\Im(\overline{z_0}e^{i\delta_v})}{(1-\lambda)ds/d\lambda + \Re(\overline{z_0}e^{i\delta_v})}\right) \tag{3.6}$$

where s is the arc length coordinate of the vortex line starting from the wedge apex.

For the vortex sheet given by the function $\delta_v(s)$, its position in the similarity plane

can be determined by the following equation

$$z_0(s) = \int_0^s e^{i\delta_v(s')} ds' \tag{3.7}$$

The image function $\zeta_0 = \zeta^{-1}(z_0)$ in the parameter plane, where $\zeta^{-1}(z)$ is the inverse mapping function, is determined from the following differential equation

$$\frac{d\zeta_0}{dz_0} = \frac{1}{(dz/d\zeta)_{\zeta=\zeta_0}}. \tag{3.8}$$

When the functions $\delta_v(s)$, $z_0(s)$ and $\zeta_0 = \zeta^{-1}(z_0)$ are found, the variation of the circulation along the vortex sheet, $\lambda(s)$, is obtained from the internal iteration procedure involving (3.4) and (3.5) only. New approximation for the function δ_v is then obtained from (3.3) and (3.6)to continue the iterations.

When solving (3.5) and (3.6) we may use the method in Smith (1968) which was also adopted by Pullin (1978) for flow passing the tip of a wedge in the unbounded fluid domain. The method divides the spiral vortex sheet which turns infinitely about a centre z_E into two parts. The first external part is the vortex sheet with $0 < \lambda < \lambda_m$, where $(1-\lambda_m)J$ is the circulation at the end point of this part, and the second inner part with $\lambda_m < \lambda < 1$ for which the circulation $(1-\lambda_m)J$ is lumped into an isolated concentrated vortex at point z_E, or at point ζ_E in the parameter plane.

In the discrete form, the solution is sought on a set of points s_i, $i = 1, ..., M$ distributed along the spiral, the initial shape of which is chosen as

$$\delta_{vi} = \begin{cases} \delta_{v0} + \delta_{vM_1}(s_i/s_{M_1})^{0.25}, & i = 1, ..., M_1 \\ \delta_{vM_1} + 2\pi N_c[(s_i - s_{M_1})/(s_M - s_{M_1})]^2, & i = M_1 + 1, ..., M. \end{cases} \tag{3.9}$$

to get a tight spiral, as suggested by Pullin (1978). Here, $\delta_{v0} = \beta_L - \pi$, N_c is the number of coils of the sheet, s_M is the length of the spiral, and points $s_i = s_M[1 - \cos(\pi/2(i-1)/(M-1))]$ are distributed in such a way to provide higher density of the points s_i close to the apex. The angle δ_{M_1} value M_1 determining the intermediate length s_{M_1} and the total spiral length, s_M vary depending on the flow configuration. The initial length of the spiral varies in the range $s_M = (0.05 - 0.5)l_O$, depending on the angles δ_h, α and γ_∞. Here, l_O is the wetted length of the leeward side of the wedge. The initial points z_{0i} and ζ_{0i} are set from (3.7) and (3.8)

The position of the lumped isolated vortex is determined from the centroid of the last coil of the sheet, i.e.

$$z_E = \frac{1}{s_M - s^*} \int_{s^*}^{s_M} z_0(s') ds', \tag{3.10}$$

where arc length coordinate s^* is chosen to satisfy the equation $\delta_{vM} - \delta_v(s^*) = 2\pi$. By following Pullin (1978), the integral in (2.33) may be approximated as

$$\begin{aligned} \left(\frac{dw}{dz}\right)_{ind} = \frac{(\zeta_0(\lambda) - c)^{2\alpha/\pi - 1}}{f_z(\zeta_0)} \Bigg[& \left.\frac{dw_1}{d\zeta}\right|_{\zeta=\zeta_0} \\ & - \frac{J}{2\pi i} \sum_{j=1}^{M} \int_{\lambda_{j-1}}^{\lambda_j} \left(\frac{1}{\zeta_0 - \zeta_0(\lambda')} - \frac{1}{\zeta_0 - \overline{\zeta_0}(\lambda')} - \frac{1}{\zeta_0 + \overline{\zeta_0}(\lambda')} + \frac{1}{\zeta_0 + \zeta_0(\lambda')} \right) d\lambda' \\ & - \frac{J(1-\lambda_M)}{2\pi i} \left(\frac{1}{\zeta_0 - \zeta_E} - \frac{1}{\zeta_0 - \overline{\zeta_E}} - \frac{1}{\zeta_0 + \overline{\zeta_E}} + \frac{1}{\zeta_0 + \zeta_E} \right) \Bigg]. \end{aligned} \tag{3.11}$$

Each of the M integrals are evaluated at midpoints $\zeta_0^{k-1,k} = (\zeta_0^{k-1} + \zeta_0^k)/2$ using the

trapezoidal rule. The Cauchy principal value of the integral at $j = k$ in the first term is of higher order as $1/(\zeta_{k-1,k} - \zeta_0)/2$ is an odd function, and it can then be ignored as it is a higher order term.

An under relaxation procedure is adopted to achieve the convergence of the iteration process determining the slope of the sheet. At the $k+1$ iteration, we have

$$\overline{\delta}_{vi}^{k+1} = r\delta_{vi}^{k+1} + (1-r)\delta_{vi}^{k}, \tag{3.12}$$

where the relaxation parameter is chosen in the range from $r = 0.001 \div 0.01$. Then, the shape of the vortex sheet at the $(k+1)^{th}$ iteration is obtained as

$$z_{0i}^{k+1} = z_{0i}^{k} + \exp[i(\overline{\delta}_{vi}^{k+1} + \overline{\delta}_{vi-1}^{k+1})/2](s_i^k - s_{i-1}^k), \tag{3.13}$$

and the arc length of each segment $s_i^{k+1} - s_{i-1}^{k+1}$ of the sheet is determined from $s_i^{k+1} = s_{i-1}^{k+1} + |z_{0i}^{k+1} - z_{0i-1}^{k+1}|$. At each k^{th} iteration of the vortex sheet, the parameters λ_i^k are determined from (3.4) and (3.5).

3.2. *Convergence of the numerical method*

The solution of the system of integral equations (2.20) and (2.24) is obtained with the number of nodes $N = 100$ on the free surface, and $M = 700$ on the vortex sheet. These two numbers have been found sufficiently large through comparison with the results from $N = 200$ and $M = 1400$. The convergence process of the solution for $2\alpha = 60^\circ$ and $2\delta_h = 20^\circ$ is shown in figure 2. Iteration starts from the initial shape given by (3.9) with $M_1 = M/4$ and $\delta_{vM_1} = \beta_R$. The inner part of the vortex sheet is chosen to be tight and is expected to expand during the iteration. It can be seen that after 1500 iterations the rings have expanded and the shape of the inner spiral part becomes more elliptical than circular. The shapes at $k = 13000$ and 26000 almost coincide as can be seen form figure 2*b*. A large number of iterations is required due to the small value of the relaxation parameter $r = 0.001$ chosen to prevent self crossing of the vortex sheet, which can lead to the breakdown of the calculation.

The number of coils of the vortex sheet, N_c is another parameter of the numerical procedure. It should be chosen large enough to minimize the effect of approximation of the inner part of the vortex sheet by lumping vortex at the centre of the spiral. In figure 3 are shown the shape of the vortex sheets and pressure distribution on the wedge sides corresponding to $N_c = 4, 5$ and 6. The sheet shapes are in good agreement overall. Some difference may be still visible when approaching to the centre of the spiral. This is obviously caused by the truncation of the coil number, and larger error is expected at the place where the truncation is made. The difference of the sheet shape near the coil centre does not have visible effect on the pressure distribution. In fact the pressure distributions from $N_c = 5$ and 6 are almost the same, as can be seen in figure 3*b*. In further computations $N_c = 5$ is chosen, which is satisfactory for the purpose of the study below.

The behaviour of the vortex strength, in the form of $\gamma' = -d\lambda/ds$, and velocity magnitudes on both sides of the sheet are shown in figure 4 as the functions of the polar angle χ about the centre of the spiral (point E) measured from $x-$axis. It can be seen that these results exhibit the oscillatory behaviour. As may be seen in the figure, at the maxima of the sheet strength the velocity magnitudes on both sides of the sheet take its minima values, while at the minima of the sheet strength, the velocity magnitudes reach its maxima values. The same behaviour was observed by Pullin (1978) for the flow over the wedge without free surface. Following Moore (1975), Smith (1968) and Pullin (1978) where details can be found, the oscillatory behaviour of vortex strength is also

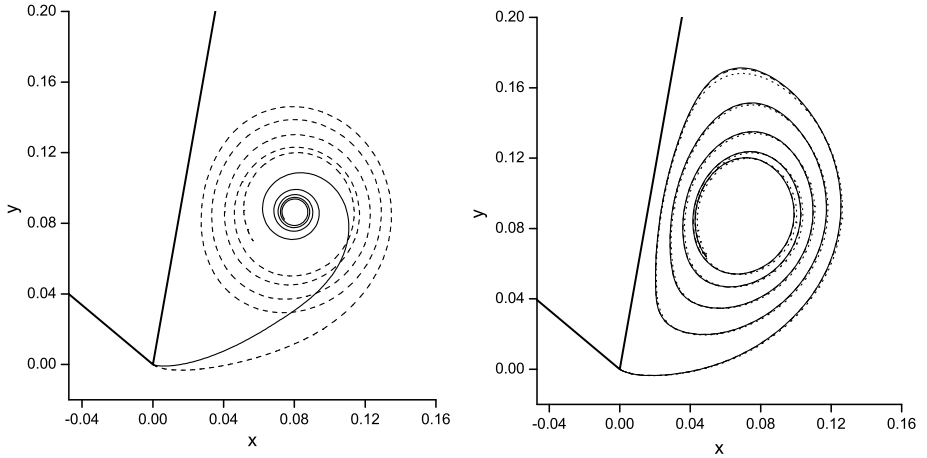

(*a*) (*b*)

FIGURE 2. Convergence of the vortex sheet for the wedge $2\alpha = 60^\circ$ and the heel angle $\delta_h = 20^\circ$: (*a*) the initial shape (solid line) and after $k = 1500$ iterations (dashed line); (*b*) the same for $k = 6000$ (dotted line), $k = 13000$ (dashed line) and $k = 26000$ (solid line).

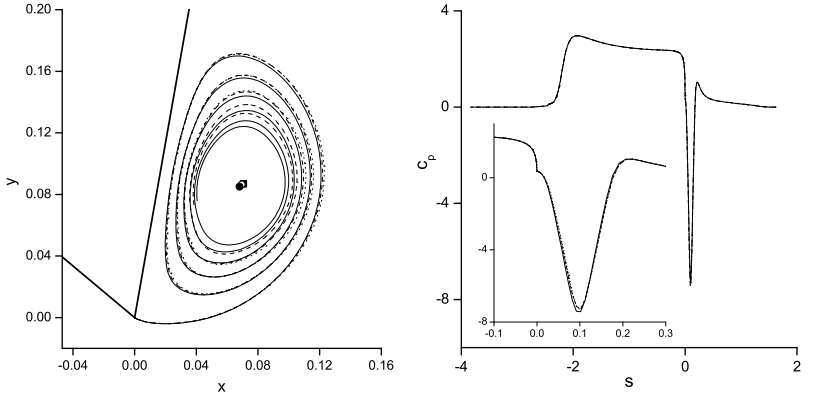

(*a*) (*b*)

FIGURE 3. Effect of the coils number, N_c, (*a*) on the shape of the vortex sheet and (*b*) the pressure distribution for the wedge angle $2\alpha = 60^\circ$ and the heel angle $\delta = 20^\circ$: $N_c = 6$, $J = 0.354$, $\lambda_M = 0.684$ (solid line and solid circle); $N_c = 5$, $J = 0.355$, $\lambda_M = 0.654$ (dashed line and opened circle); $N_c = 4$, $J = 0.355$, $\lambda_M = 0.592$ (dotted line and solid square.)

related with the shape of the sheet which exhibits ellipticity that may be defined as the ratio of the largest radius to the smallest one over one complete turn. This may be seen in figure 3 and in other results given below.

3.3. *Numerical results for asymmetric water entry of the wedges*

In the context of figure 1*a*, the flow is symmetric with respect to axis of the wedge for $\gamma_\infty = 90^\circ$ and $\delta_h = 0$, and is asymmetric in all other cases. The wedge heel angle may vary in the range bounded by some constraints. For a positive δ_h, the deadrise angle on the left hand side, $\pi - \beta_L > 0$, should remain to be positive, or $\pi/2 - \alpha - \delta_h > 0$. For the deadrise angle on the right hand side of the wedge, β_R, it should be less than a critical angle β_R^*, beyond which the fully attached solution, or the leeward side remain in contact with water, might not exist or might not be physical. Semenov & Yoon (2009)

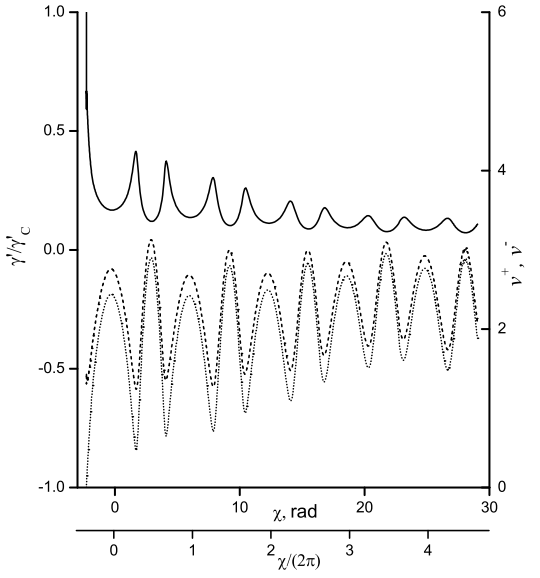

FIGURE 4. Variation of vortex strength along the vortex sheet (solid line) and velocity magnitude on the $'+'$ (dashed line) and $'-'$ sides of the sheet for the case shown in figure 3
.

found that the critical angle $\beta_R^* = \gamma_\infty \pm \Delta$, where the value Δ is in the order of a few degrees, and its exact value depends on the flow configuration. If we use $\beta_R^* \approx \gamma_\infty$ then the constrain is $\alpha - \delta_h > 0$ for the case of vertical entry, and the range of the heel angles is approximately $0 < \delta_h < \alpha$.

The free streamlines and vortex sheet for the wedge angle $2\alpha = 30°$ are shown in figure 5 for the heel angles $\delta_h = 5°$ and $14.2°$. The second case corresponds approximately to the limit heel angle β_R^*. The enlargement near the apex clearly shows the streamline separation from the wedge apex and the spiral vortex sheet. There are also two stagnation points. One is point A on the windward side as shown in figure 1a, from which the zero streamline splits and one of them moves towards the wedge apex and then separates from the apex, enclosing the re-circulation region. The other stagnation point occurs on the leeward side. This is generated by reattachment of the zero streamline the wedge side. The zero streamline and some of the closed streamlines inside the re-circulation region almost coincides with some parts of the vortex sheet line. In fact the zero streamline leaves windward side tangentially, which is the same as the vortex sheet. Along the streamline its normal velocity is zero by definition. From (3.4) and (2.45), we can have the velocity normal to the vortex line near the apex and it tends to zero at the apex. This leads to that two lines almost coincide near the apex, as shown in figure 5. In fact figure 5 further shows that these two lines remain close to each other until it becomes close to the leeward surface of the wedge. This suggests that the normal velocity of the vortex sheet has remained to be small. Near the body surface, the zero streamline reattaches to the wedge surface while the vortex line bends to form a spiral line. For flow without the vortex sheet Semenov & Wu (2012), the zero streamline will always stay on the body surface even when it turns at the wedge apex. There are no closed streamlines and the streamlines near $y-$axis from $y = -\infty$ will bend near the wedge apex and then move to $y = \infty$.

The size of the spiral vortex region in figure 5b for the heel angle $\alpha = 14.2°$ is about

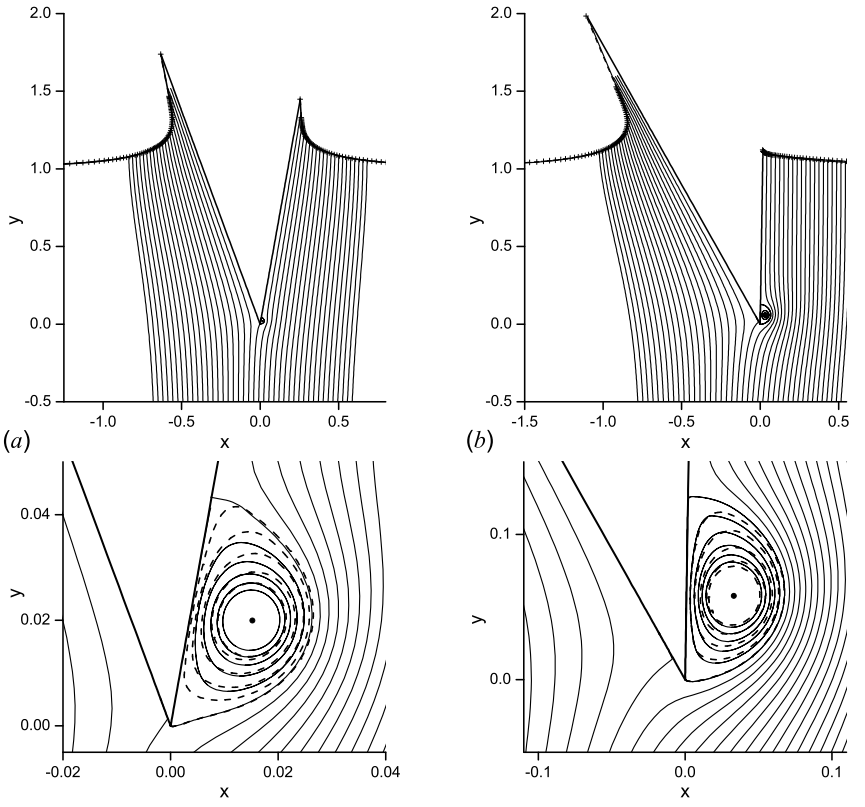

FIGURE 5. Streamline pattern (solid line) and the vortex sheet (dashed line) for the wedge $2\alpha = 30°$: (a) $\delta_h = 5°$, $J = 0.064$, $\lambda_M = 0.257$ and (b) $\delta_h = 14.2°$., $J = 0.429$, $\lambda_M = 0.431$

twice larger than that in figure 5*a* for $\alpha = 5°$. The distance between the stagnation point on the windward side and the wedge apex is also larger in the latter. This is clearly because the flow will be more asymmetric at large δ_h. A large cross flow then leads to a larger circulation. This is reflected in figure 5 by $J = 0.064$ for case (a) and $J = 0.429$ for case (b). A common feature for both cases in figure 5 is that the size of the spiral vortex region is much smaller than the wetted length of the leeward side of the wedge. This is because even though the magnitude of the velocity leaving the windward in (2.45) may be comparable with the entry speed, especially in case (*b*), it turns very fast and forms a spiral with small radius. As the vortex sheet is far away from the free surface, its effect on the free surface is rather small. In figure 5 the free surface for the flow with vortex sheet is shown by the solid line, while for the attached flow without vortex sheet it is shown by the dashed line with symbols. The difference between them is hardly visible, and they virtually coincide.

In figure 6 the pressure distributions on the wedge corresponding to the flow with and without vortex sheet are compared for the cases shown in figure 5. It is clearly seen that pressure distributions coincide almost everywhere except a small region near the apex. Together with its small effect on the free surface previously, the effect of the spiral vortex is very much limited to the local area. However, precisely in the local area near the apex, the presence of the vortex sheet is crucial. It has completely changed flow pattern, discussed previously. Here the vortex-free solution gives infinite pressure at the apex, or the solution is singular there. The inclusion of the vortex sheet removes this unphysical

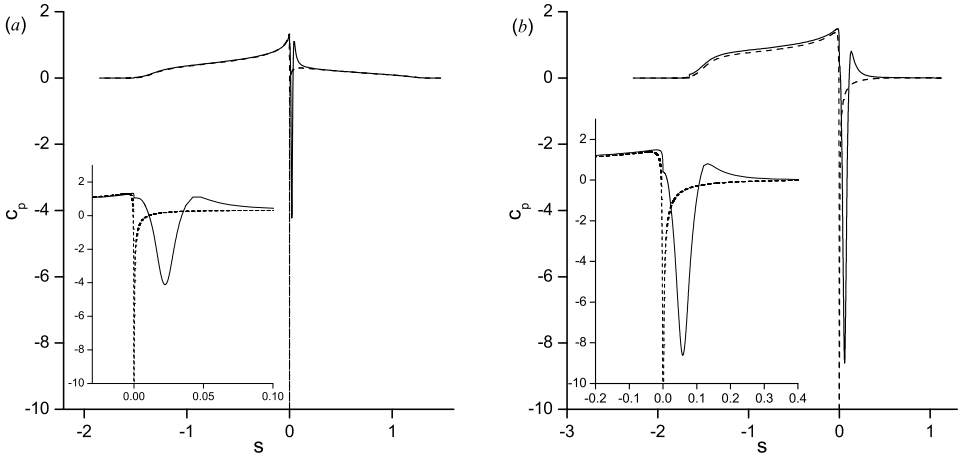

FIGURE 6. Pressure coefficient along the left ($s < 0$) and right ($s > 0$) hand sides of the wedge for the wedge $2\alpha = 30°$: (a) $\delta_h = 5°$ and (b) $\delta_h = 14.2°$. The dashed lines correspond to the flow model without vortex sheet.

singularity, and the pressure at the apex becomes finite, as shown in figure 6 for both cases. In the enlargement it can be seen as s increases from $s = 0$ on the leeward side, the pressure drops to its minimal value and then increases. From the analysis of the results it is found that the point of the minimal pressure coefficient is close to the location at a normal distance closest to the centre of the spiral. By comparing figure 6 a) and b) it is seen that the larger heel angle, the larger drop of the local pressure on the leeward side occurs.

In figure 6 b), the vortex free solution with singularity at the apex (dashed line) predicts negative pressure coefficient on the whole leeward side ($s > 0$) of the wedge. We should notice that this is in the context that $\delta_h = 14.2°$ corresponds to the limit discussed above. In contrast of this, the solution with vortex sheet predicts local positive maximum near the stagnation point on the leeward side of the wedge, where the zero streamline reattaches the body surface at the right angle, which can be seen through the enlargement of the streamline patterns in figure 5b. The pressure on the leeward side is very sensitive to the heel angle near its limit value. Therefore, a slight increase of the heel angle further decreases the pressure coefficient rapidly, making the pressure coefficient negative along the whole leeward side of the wedge. In such a case no converged solutions could be obtained. For wedge angles $2\alpha = 60°$ and $90°$ the free surface shape and streamline patterns are shown in figure 7. For the larger wedge and heel angles, the stagnation point on the windward side moves further away from the apex. There is also a larger cross flow at the wedge apex. This results in a larger size of the separation region with a larger overall circulation on the leeward side. The shape of the closed streamlines inside the separated zero streamline look similar in figure 7(a) and (b), but the radius is larger for the larger heel angle. The effect of the vortex sheet on the free-surface shape remains to be small and the difference between the solutions with and without vortex sheet is virtually invisible. In figure 8 are shown the pressure distributions on the wedge for the cases shown in figure 7. For the larger wedge and heel angles the pressure drops rapidly on the leeward side and reaches its minimum near the centre of the spiral. Away from apex, the pressure distribution virtually coincides with that obtained from the previous solution of water-entry problem without vortex sheet (Semenov & Wu (2012)).

The values of the pressure coefficient at the apex, c_{pC}, minimal pressure on the leeward

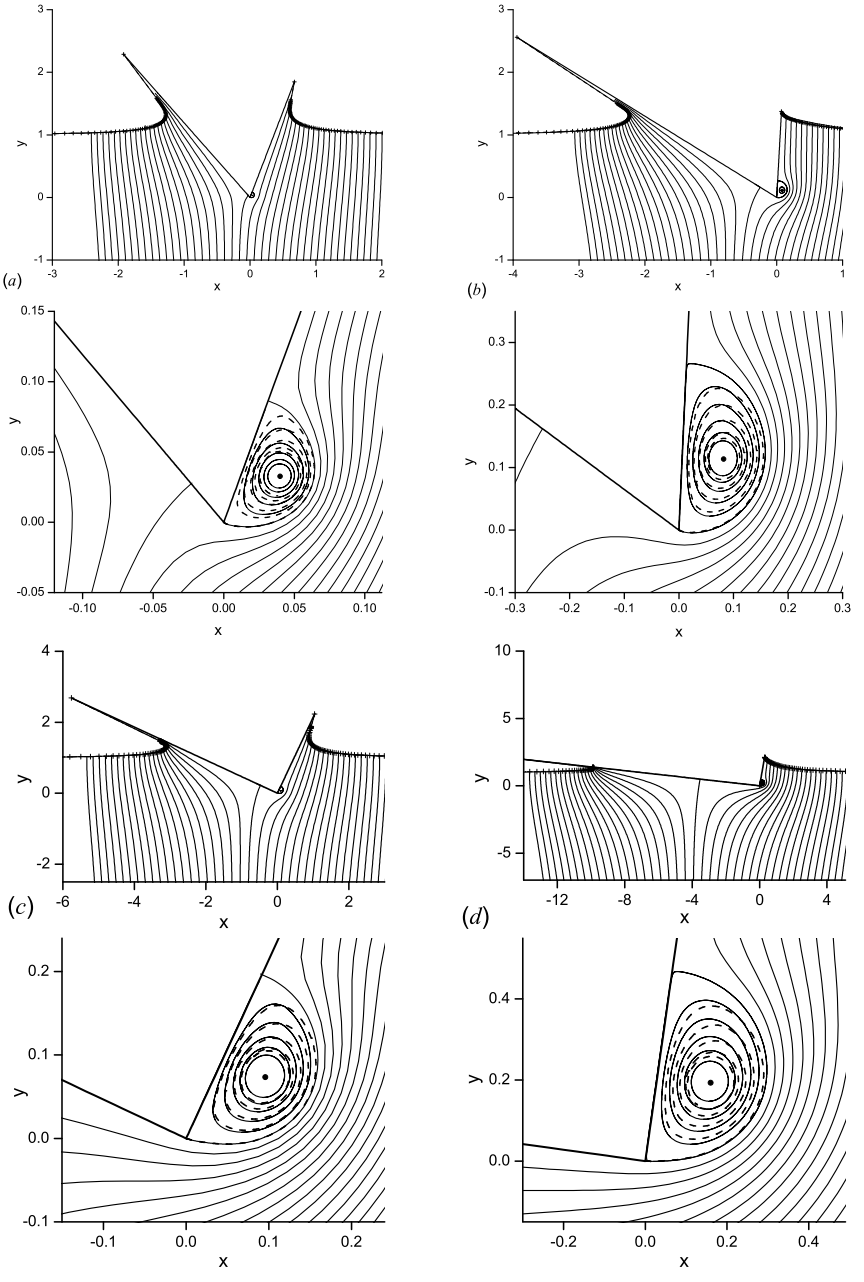

FIGURE 7. Streamline pattern (solid line) and the vortex sheet (dashed line) for the wedge angles: $2\alpha = 60^\circ$ (a) $\delta_h = 10^\circ$, $J = 0.083$, $\lambda_M = 0.436$ and (b) $\delta_h = 27^\circ$, $J = 0.724$, $\lambda_M = 0.592$; $2\alpha = 90^\circ$ (c) $\delta_h = 20^\circ$, $J = 0.169$, $\lambda_M = 0.535$ and (d) $\delta_h = 37^\circ$, $J = 0.801$, $\lambda_M = 0.627$.

side of the wedge, $c_{p\min}$, the total circulation, J, and the parameter λ_M are shown in Table 1 for wedges of different inner angles and heel angles. It can be seen from the table that the pressure coefficient at the wedge apex and the minimal pressure coefficient on the lee-ward side decreases while the total circulation increases as the heel angle increases.

The force on the wedge are evaluated through integration of the pressure distribution

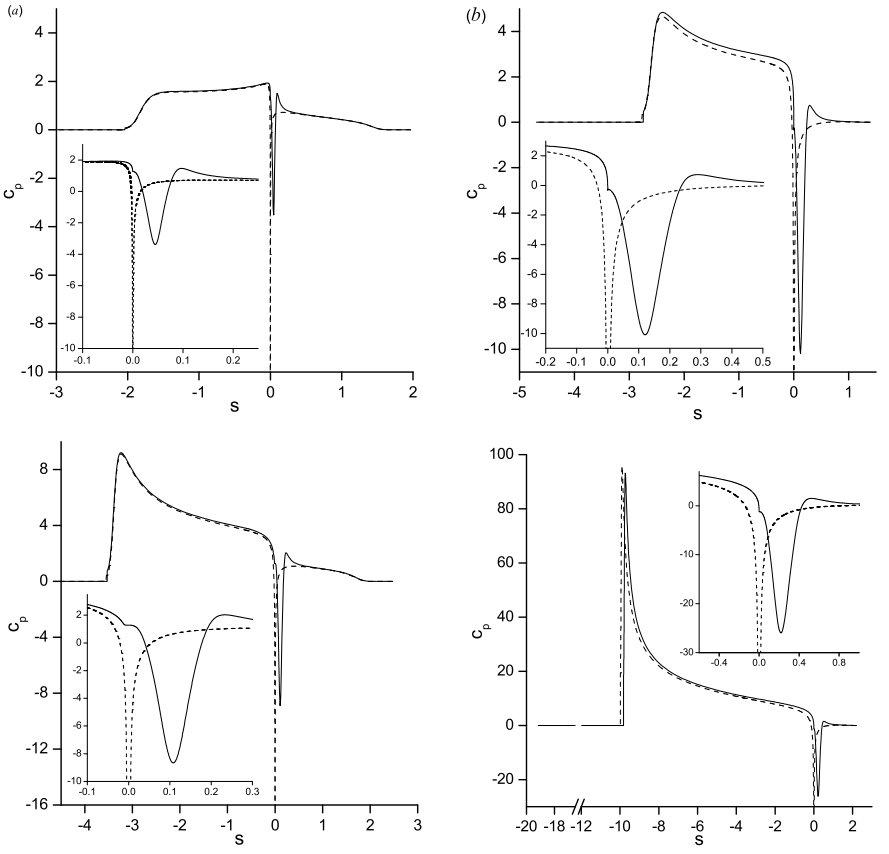

FIGURE 8. Pressure coefficient along the windward ($s < 0$) and and leeward ($s > 0$) sides of the wedge at $2\alpha = 60^\circ$, (a) $\delta_h = 10^\circ$ and (b) $\delta_h = 27^\circ$. The dashed lines correspond to the flow model without vortex sheet.

2α	δ_h	c_{pC}	$c_{p\,\min}$	J
30	0	1.30	-	0
30	5	1.06	-5.80	0.0637
30	10	0.785	-7.10	0.181
30	14.2	0.398	-8.90	0.429
60	0	1.780	-	0
60	10	1.28	-3.51	0.0826
60	20	0.442	-6.36	0.336
60	27	-0.253	-10.2	0.724
90	0	2.71	-	0
60	10	2.20	-2.33	0.0397
90	20	1.29	-8.75	0.169
90	30	0.320	-16.5	0.415
60	37	-1.23	-26.2	0.801

TABLE 1. Some detailed results for vertical water entry of various wedges.

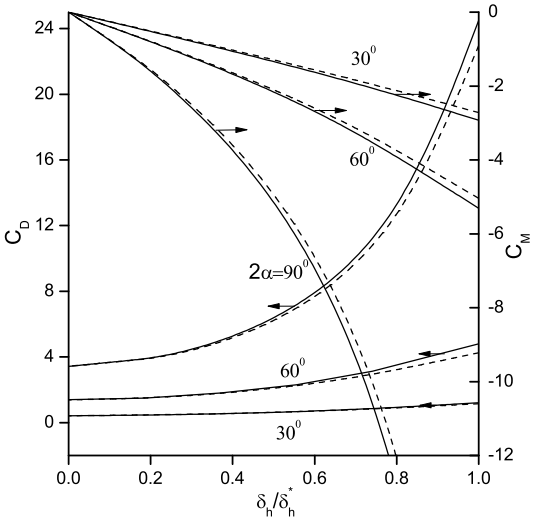

FIGURE 9. Drag force coefficient (left axis) and moment about the wedge apex (right axis) versus normalized heel angle δ_h/δ_h^*, where $\delta_h^* = 14.2^\circ$, 27° and 37° for the wedge angles $2\alpha = 30^\circ$, 60° and 90°, respectively. The solid and dashed lines correspond to results with and without vortex sheet respectively.

along its sides. The drag is defined as the force component along the incoming velocity direction. Its coefficient, C_d, can be written as:

$$C_D = C_R \sin(\gamma_\infty - \beta_R) + C_L \sin(\beta_L - \gamma_\infty) \tag{3.14}$$

where

$$C_{\{R,L\}} = \frac{2}{\rho V_y^2 H^2} \int_0^{V_{\{O,B\}}t} P(S)dS = \frac{1}{h} \int_{\{0,c\}}^{\{c,\infty\}} c_p[s(\xi)]d\xi,$$

are the coefficients of the forces normal to the right and left hand sides of the wedge, respectively. The y-component of the incoming velocity, or $V_y = V \sin\gamma_\infty$ has been used as a reference velocity. The moment coefficient, C_M, about the wedge apex is

$$C_M = \frac{2}{\rho V_y^2 H^2} \int_0^{V_O t + V_B t} (S_O - S)P(S)dS = \frac{1}{h^2} \int_0^\infty (v_0 - s)c_p[s(\xi)]\frac{ds}{d\xi}d\xi, \tag{3.15}$$

where

$$H = V_y th, \qquad S_O = v_0 Vt, \qquad h = \sin\gamma_\infty[\cot\beta_R + \cot\beta_L], \qquad c_p = \frac{2(P - P_a)}{\rho V_y^2 \sin\gamma_\infty}.$$

It can be seen from figure 9 that the vortex sheet also has a small effect on the force coefficients. This is of course expected taking into account that the effect of the vortex sheet on the pressure distribution is very much localized.

The free surface shape and streamline patterns are shown in figure 10 for the case of oblique entry at $2\alpha = 90^\circ$ and $2\alpha = 120^\circ$. The wedges are symmetric about the $y-$axis. The stagnation point on the windward side can be clearly seen, and it moves further away from the apex for the larger oblique angles. The cross flow over the apex creates separation region similar to that observed for vertical entry of the heeled wedge. For the wedge of angle $2\alpha = 90^\circ$ the inflow velocity angle $\gamma = 45^\circ$ is close to the limit oblique angle for which the attached solution might be found. For larger oblique angle, or larger

2α	γ_∞	c_{pC}	$c_{p\,\min}$	J
90	90	2.70	-	0
90	80	2.36	0.229	0.211
90	70	2.08	-4.75	0.399
90	60	1.40	-11.3	0.737
90	50	0.724	-15.5	0.973
90	45	-0.291	-20.9	1.245
120	90	4.59	-	0
120	80	4.29	4.21	0.199
120	70	3.87	3.76	0.444
120	60	3.48	-3.54	0.628
120	50	3.03	-12.3	0.773
120	40	1.79	-19.9	1.026
120	30	0.907	-48.5	1.303

TABLE 2. Some detailed results for oblique water entry of various wedges.

horizontal component of the velocity the separation region becomes larger. However, its size remains relatively small in comparison with the wetted length of the wedge. Similar results are shown for the wedge angle $2\alpha = 120^\circ$ and the inflow velocity angles $\gamma = 70^\circ$ and 30°. The latter is close to the limit oblique angle. At a given wedge angle the size of the separation region increases as the horizontal component of the inflow velocity increases, and it becomes largest at the limit oblique angle γ_∞. The size is of course also affected by the wedge angle itself. If we compare these two limiting cases in figure 10, (cases (b) and (d)), it can be seen that the size of separation region for the wedge of angle $2\alpha = 90^\circ$ at $\gamma = 45^\circ$ is about twice of that for $2\alpha = 120^\circ$ at $\gamma = 30^\circ$. It is partly because the effort for the flow to turn around apex decreases when the wedge angle $2\alpha \to 180^\circ$, while it is also related to γ_∞. The pressure distributions corresponding to the cases in figure 10 are shown in figure 11. In all the cases the effect of the vortex sheet is localized near the apex, and away from the apex the pressure almost coincides with that corresponding to the attached flow.

The pressure coefficient at the apex and the minimal pressure coefficient on the leeward side as well as the total circulation are shown in Table 2.

4. Conclusions

The problem of asymmetric flow due to water-entry of the wedge with the rolled-up vortex sheet shed from the apex is considered. The integral hodograph method has been employed to determine in an explicit form the complex potential and the flow singularities corresponding to vortex-free flow. This provides an incoming flow for the vortex sheet shed from the wedge apex, whose solution is obtained from the Birkhoff-Rott integral equation which determines the vortex sheet dynamics. Numerical results are obtained for wedges of a range of inner, heel and oblique angles.

The obtained flow patterns show the formation of the recirculation/separation region with a stagnation point on the leeward side of the wedge due to the reattachment of the streamline shed from the apex to the body surface. The size of the separation region is estimated based on the area bounded by the zero streamline linking the wedge apex and the stagnation point on the leeward side. The region inside this streamline increases when the overall flow is more asymmetric and the velocity at apex on the windward side

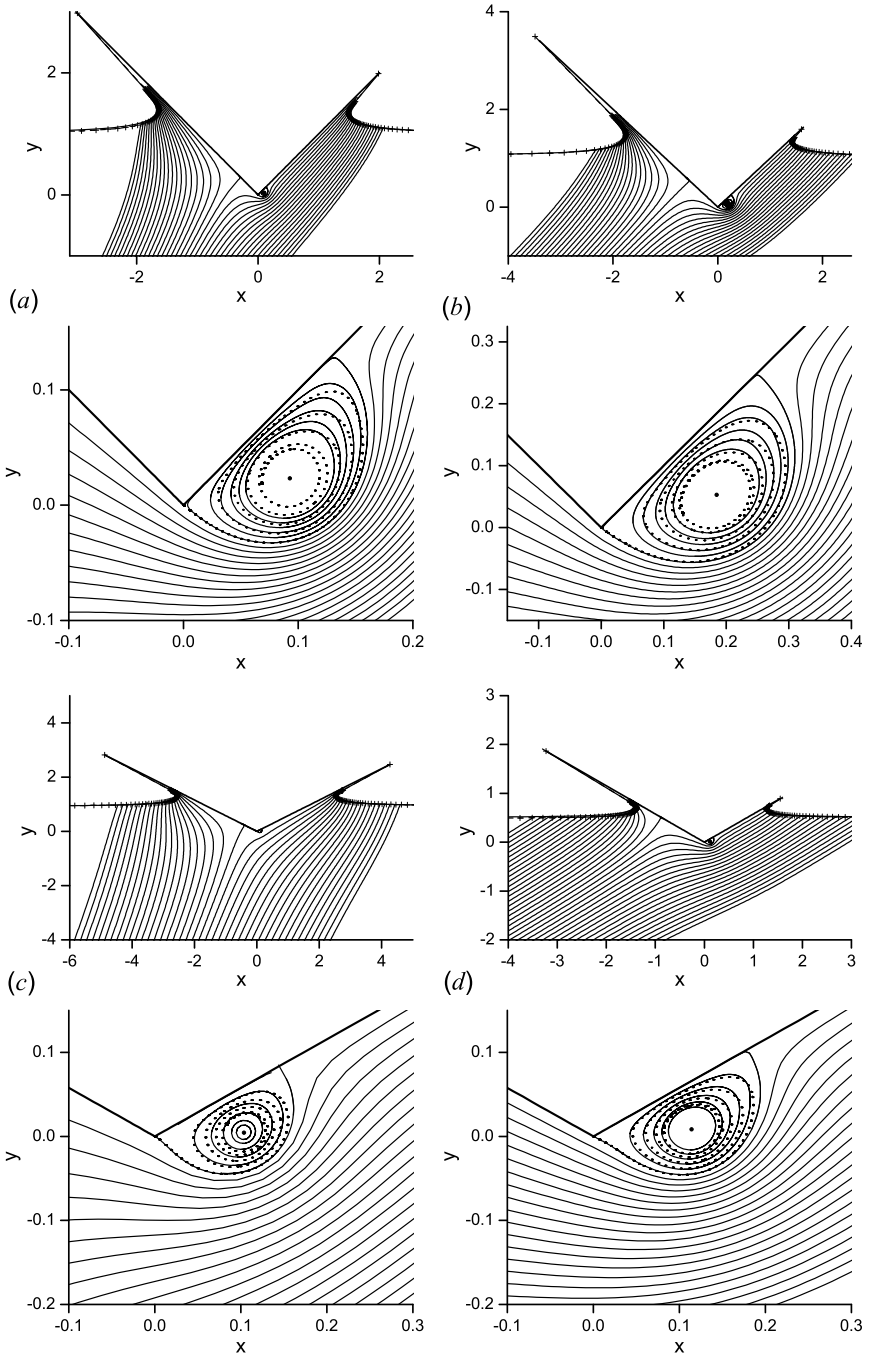

FIGURE 10. Streamline pattern (solid line) and the vortex sheet (dashed line) for the oblique water-entry of the wedge: $2\alpha = 90^\circ$ (a) $\gamma_\infty = 60^\circ$, $J = 0.737$, $\lambda_M = 0.477$ and (b) $\gamma_\infty = 45^\circ$, $J = 1.245$, $\lambda_M = 0.600$; $2\alpha = 120^\circ$ (c) $\gamma_\infty = 70^\circ$, $J = 0.444$, $\lambda_M = 0.629$ and (d) $\gamma_\infty = 30^\circ$, $J = 1.303$, $\lambda_M = 0.512$.

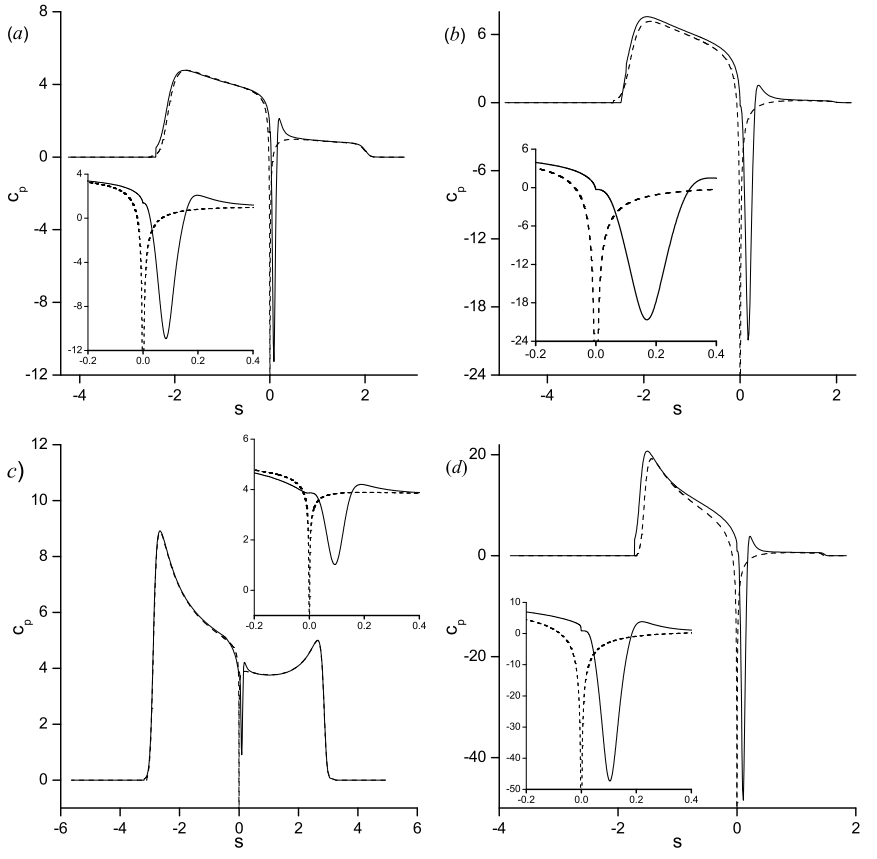

FIGURE 11. Pressure distribution along the windward ($s < 0$) and and leeward ($s > 0$) sides of the wedge for oblique entry at $2\alpha = 90^\circ$, (a) $\gamma_\infty = 60^\circ$ and (b) $\gamma_\infty = 45^\circ$, and $2\alpha = 120^\circ$, (c) $\gamma_\infty = 70^\circ$ and (d) $\gamma_\infty = 30^\circ$. The dashed lines correspond to the flow model without vortex sheet.

becomes larger. However, the size of the separation region is relatively small, compared with the wetted length of the leeward side of the wedge. Thus the vortex sheet has small effect on the free surface and its principal effects are on the velocity and the pressure near the apex, as well as the flow configuration inside the flow separation region. The vortex sheet removes the singularity in the attached flow solution, leading to a finite pressure and velocity at the apex. The location of the minimal pressure is found to be on the leeward side of the wedge near the apex, and is near the point with minimal distance to the centre of the spiral sheet.

The vortex sheet shed from the apex exhibits a shape more elliptical than circular, which is similar to that found by Pullin (1978) for flow past a wedge in an unbounded fluid domain without the free surface. The vortex strength along the spiral sheet undergoes an oscillatory process together with the velocity magnitudes on the both sides of the sheet, and the magnitudes of their oscillations decay toward the centre of the spiral.

This work is supported by Lloyd's Register Foundation (LRF) through the joint centre involving University College London, Shanghai Jiaotong University and Harbin Engineering University, to which the authors are most grateful. LRF supports the advancement of engineering-related education, and funds research and development that enhances safety of life at sea, on land and in the air.

REFERENCES

Armand, J. L. & Cointe, R. 1987 Hydrodynamic impact analysis of a cylinder. *J. Offshore Mech. Artic Engng* **9**, 237–243.

Birkhoff, G. 1962 Helmholtz and Taylor instability. *In Proc. Sympos. Appl. Math.*, **XIII**, 55-76. Providence, R.I.

Chekin, B.S. 1989 The entry of a wedge into incompressible fluid. *Prikl. Matem. Mekhan.* **53**, pp. 300–307.

Dobrovol'skaya, Z.N. 1969 Some problems of similarity flow of fluid with a free surface. *J. Fluid Mech.* **36**, 805–829.

Faltinsen, O. M. 2005 *Hydrodynamics of High-speed Marine Vehicles.* 454p. Cambridge University Press.

Fraenkel, L. E. & McLeod, J. B. 1997 Some results for the entry of a blunt wedge into water. *Phil. Trans. R. Soc. London A.* **355**, 523–535.

Gakhov, F.D. 1990 *Boundary Value Problems.* 561p. Dover Publication Inc.

Gurevich, M. I. 1965 *Theory of jets in ideal fluids.* Academic Press, 585p.

Howison, S. D., Ockendon, J. R. & Wilson, S. K. 1991 Incompressible water - entry problems at small deadrise angles. *J. Fluid Mech.* **222**, 215 – 230.

Howison, S. D., Ockendon, J. R. & Oliver, J. M. 2004 Oblique slamming, planing and skimming. *J. Engng Maths.* **48**, 321–337.

Judge, C., Troesch, A. & Perlin, M. 2004 Initial water impact of a wedge at vertical and oblique angles. *J. Eng. Math.* **48**, 279 – 303.

Iafrati A. 2000 Hydrodynamics of Asymmetric Wedges Impacting the Free Surface. *European Congress on Computational Methods in Applied Sciences and Engineering. ECCOMAS 2000.* Barselona, 11-14 Sept.

Jones, M. A. 2003 The separated flow of an inviscid fluid around a moving flat plate. *J. Fluid Mech.* **496**, 405 – 441.

Joukovskii, N.E. 1890 Modification of Kirchhof's method for determination of a fluid motion in two directions at a fixed velocity given on the unknown streamline. *Matemat. sbornik* **XV** (in Russian).

von Karman, T. 1929 The impact of seaplane floats during landing. *Washington, DC:NACA Tech. Note 321.*

Korobkin, A.A., & Puknachov, V.V. 1988 Initial Stage of Water Impact. *Ann. Rev. Fluid Mech.* 159 -185.

Korobkin, A. A. 2004 Analytical models of water impact. *Eur. J. Appl. Maths.* **15**, 821–838.

Mei, X., Liu, Y. & Yue, D.K.P. 1999 On the water impact of general two-dimensional sections. *Appl. Ocean Res.* **21**, 1-15.

Michell, J.H. 1890 On the theory of free stream lines. *Phil. Trans. Roy. Soc. A.* **181** DOI: 10.1098/rsta.1890.0006.

Moore, D. W. 1975 The rolling up of a semi-infinite vortex sheet. *Proc. Roy. Soc. A.* **345**.

Oliver, J.M. 2007 Second-order Wagner theory for two-dimensional water-entry problems at small deadrise angles. *J. Fluid Mech.*, **572**, pp. 59 – 85.

Pullin, D. I. 1978 The large-scale structure of unsteady self-similar rolled-up vortex sheets. *J. Fluid Mech.* **88**(03), 401 – 430.

Riccardi, G. & Iafrati, A. 2004 Water impact of an asymmetric floating wedge. *J. Engn Math.* **49**, 19 – 39.

Rott, N. 1956 Diffraction of a weak shock with vortex generation. *J. Fluid Mech.*, **1**(1), pp. 111 – 128.

Saffman, P.G. 1993 *Vortex Dynamics.* 326p. Cambridge University Press.

Semenov, Y. A. & Iafrati, A. 2006 On the nonlinear water entry problem of asymmetric wedges. *J. Fluid Mech.* **547**, 231 – 256.

Semenov, Y. A. & Yoon, B-S. 2009 Onset of flow separation for the oblique water impact of a wedge. *Phys. of Fluids* **21**, 112103.

Semenov, Y.A. & Wu, G.X. 2012 Asymmetric impact between liquid and solid wedges. *Proc. Roy. Soc. A.* **469**. DOI: 10.1098/rspa.2012.0203.

Smith, J. H. B. 1968 Improved calculations of leading edge separation from slender delta wings. *Proc. Roy. Soc. A.* **306**, 87–90.

Xu., L. 2016 Numerical study of viscous starting flow past wedges. *J. Fluid Mech.* **801**, 150-165.

Xu, G.D., Duan, W.Y., & Wu, G.X. 2008 Numerical simulation of oblique water entry of an asymmetrical wedge. *Ocean Engineering*, **35**, 1597–1603.

Xu, G.D., Duan, W.Y., & Wu, G.X. 2010 Simulation of water entry of a wedge through free fall in three degrees of freedom. *Proc. Roy. Soc. A.* **466**, 2219–2239.

Wagner, H. 1932 Über Stoßund Gleitvorgänge an der Oberfläche von Flüssigkeiten. *Z. Angew. Math. Mech.* **12**, 192–215.

Zhao, R., Faltinsen, O.M. & Aarsnes, J. 1996 Water entry of arbitrary two-dimensional sections with and without separation. *Proc.* 21^{st} *Symposium on Naval Hydrodynamics* pp. 118133. Trondheim, Norway.